Bioresource Technology Reports 21 (2023) 101325

Contents lists available at ScienceDirect

Bioresource Technology Reports

journal homepage: www.sciencedirect.com/journal/bioresource-technology-reports

Optimizing date palm leaf and pistachio shell biochar properties for antibiotic adsorption by varying pyrolysis temperature

Michael P. Schmidt *, Daniel J. Ashworth, Nydia Celis, Abasiofiok Mark Ibekwe

USDA-ARS United States Salinity Laboratory, Riverside, CA, USA

ARTICLE INFO

Keywords:
Biochar
Pyrolysis
Agricultural byproducts
Adsorption
Treatment
Antibiotics

ABSTRACT

This study implemented biochars produced from two arid agricultural byproducts, date palm leaves and pistachio shells, at pyrolysis temperatures from 400 to 800 °C to remove trimethoprim, sulfamethoxazole and sulfapyridine antibiotics from mixed solutions. By altering pyrolysis temperature and feedstock, produced biochars yielded a range of physicochemical properties resulting in distinct antibiotic adsorption. Antibiotic adsorption capacity generally decreased with increasing pyrolysis temperature, while adsorption affinities were temperature independent for trimethoprim and increased with pyrolysis temperature for sulfamethoxazole and sulfapyridine. Correlation against biochar properties suggested cation exchange capacity and functional group composition related well to adsorption capacity and polarity/hydrophobicity was linked to adsorption affinities. Antibiotic removal efficiencies by biochars from both feedstocks compared favorably against previous reports, with up to 97.6, 98.1 and 99.5 % of trimethoprim, sulfamethoxazole and sulfapyridine removed, respectively. This work relates biochar production conditions to properties and subsequent antibiotic adsorption, demonstrating application of these materials for removing antibiotics from wastewater.

1. Introduction

Irrigated agriculture accounts for about 70 % of water use globally, representing a major application of freshwater resources worldwide (Ritchie and Roser, 2022). As freshwater irrigation resources become increasingly stressed due to greater uncertainty in climate, increasing population and higher demand from energy and industrial sectors, alternative irrigation water sources are receiving greater consideration (Sapkota, 2019). This includes the use of recycled wastewater as an irrigation water source, which represents an attractive option because of its ubiquity, nutrient content and resilience against seasonal flow fluctuations (Jaramillo and Restrepo, 2017). These points are particularly relevant in arid and semi-arid growing regions, which are water-stressed and have a large proportion of the global population to generate potentially usable wastewater (Scholes, 2020). Given the previous passage of recycled wastewater through municipal and/or industrial usage chains, recycled wastewaters may contain trace levels of contaminants (e.g., personal care products, pharmaceuticals, perfluoroalkylated substances) (Fu et al., 2019; Szabo et al., 2018). Of particular risk in irrigated agricultural systems are several residual antibiotics which coexist in recycled wastewater streams. Despite the low concentrations (ng L^{-1} to μg L^{-1}) of antibiotics in treated wastewaters, evidence suggests that these concentrations are sufficient to foster antibiotic resistance in wastewater streams and soils (Kampouris et al., 2021; Kovalakova et al., 2020; Wang et al., 2020). Subsequent transfer of antibiotic resistance determinants to soil organisms and plants may occur, introducing them into the consumer food chain and further elevating exposure to humans and livestock. Removing trace levels of antibiotics from wastewater streams may therefore mitigate the risks associated with antibiotic resistance in recycled wastewater irrigated agricultural systems.

A promising strategy for immobilizing antibiotics from wastewater streams is the use of environmentally-friendly and cost-effective biochar adsorbents (Krasucka et al., 2021). Biochar is a black carbon material made from the thermochemical transformation of a biomass feedstock (e.g., manure, agricultural byproducts, food wastes) under an anoxic atmosphere (Lehmann and Joseph, 2015). Resultant biochars possess high surface areas and reactive surface functionalities that favor adsorption of several classes of contaminants, including antibiotics (Krasucka et al., 2021). These key biochar characteristics are influenced by biochar feedstock composition and pyrolysis temperature. Recent studies have shown that altering these may influence adsorption behavior toward antibiotics. For example, a study probing antibiotic

* Corresponding author at: USDA-ARS Salinity Laboratory, 450 W Big Springs Road, Riverside, CA 92507, USA.
E-mail address: mike.schmidt@usda.gov (M.P. Schmidt).

https://doi.org/10.1016/j.biteb.2022.101325
Received 3 October 2022; Received in revised form 27 December 2022; Accepted 28 December 2022
Available online 6 January 2023
2589-014X/Published by Elsevier Ltd.

adsorption onto cotton gin waste and guayule bagasse biochars pyrolyzed at 350 and 700 °C showed that cotton gin waste biochar produced at 700 °C had a greater sulfapyridine removal efficiency than biochars produced at lower temperatures and/or from guayule bagasse feedstock (Ndoun et al., 2021). The authors attribute this to an inherent lower proportion of oxygen-containing functional groups in cotton gin waste coupled with the increase in surface area and hydrophobicity of biochars produced with increasing pyrolysis temperatures, all of which enhanced the hydrophobic and π-π interactions between sulfapyridine and the biochars. Greater adsorption was generally observed with guayule bagasse biochars for erythromycin, however, which likely adsorbed through hydrophilic interaction with the biochars. Another study using manure, biosolids and coffee ground biochar to adsorb antibiotics from a mixture of seven antibiotic compounds also demonstrated the impact of feedstock on adsorption performance (Stylianou et al., 2021). Feedstock source impacted equilibrium and kinetic adsorption behavior, resulting in differences of antibiotic removal selectivity between biochars. These results highlight the potential for biochar adsorbents to remove antibiotics from wastewater streams in single solute and environmentally relevant mixed antibiotic systems. The influence of feedstock, pyrolysis temperature and target antibiotic on removal performance, however, need to be better understood to optimize adsorption given the vast number of feedstocks and production conditions available.

Economic and environmental favorability of biomass feedstocks is influenced by regional availability and feedstock establishment (Liu et al., 2017). It is therefore advantageous to select feedstocks accessible as byproducts of existing activity in arid and semi-arid regions globally when considering purification of treated wastewater to be applied in water stressed agroecosystems. Two feedstocks which fit these criteria are date palm (*Phoenix dactylifera*) leaves (DPL) and pistachio (*Pistacia vera*) nut shells (PS). Date palms, which are cultivated in arid and semi-arid growing regions globally (e.g., the Middle East and the Southwestern United States), annually produce up to 20 kg of dry biomass per tree. This includes leaflets, rachides and petioles suitable for conversion into biochar with the potential to adsorb contaminants from wastewater streams (Chao and Krueger, 2007; Mallaki and Fatehi, 2014). Specifically, DPL biochars have been demonstrated to adsorb a wide range of heavy metals and organic contaminants from solution (Sizirici et al., 2021; Tahir et al., 2020). In addition to date palms, pistachio nuts are largely cultivated in dry regions of the Middle East and Western United States (FAOSTAT). Globally, 1,125,305 t of pistachios were produced in 2020 (FAOSTAT). Of total pistachio nut weight, roughly 50 % is shell, representing a large potential source of feedstock from this byproduct (Dreher, 2012). Given this potential, PS biochars have previously been researched as adsorbents and shown to be effective for the removal of organic and heavy metal contaminants (Komnitsas et al., 2015; Komnitsas and Zaharaki, 2016). DPL and PS collectively represent biochar feedstocks associated with water-stressed agroecosystems and have demonstrated potential to remove a wide range of contaminants from aqueous solution. Due to these considerations, DPL and PS were selected as biochar feedstocks in this study.

The objective of this study is to elucidate the influence of pyrolysis temperature and the resulting characteristics of biochars produced from agricultural byproduct feedstocks on antibiotic adsorption in a mixed (multi-compound) system. This objective is addressed by producing biochars from date palm leaves and pistachio shells at three pyrolysis temperatures (400, 600 and 800 °C). Biochars were then characterized based on intrinsic (e.g., elemental composition, surface area, functional group composition) and extrinsic (e.g., cation exchange capacity, pH, surface charge) properties previously linked to antibiotic adsorption behavior. The performance of the produced biochars as adsorbents for antibiotics previously identified in treated municipal wastewater (sulfapyridine (SPY), sulfamethoxazole (SMX) and trimethoprim (TMP)) in mixed solutions is evaluated and related to biochar properties on the basis of feedstock and pyrolysis temperature. These findings will compliment future studies predicting biochar antibiotic adsorption behavior based on biochar physicochemical properties. More broadly, this work informs further efforts to develop batch and fixed-bed filtration systems for removing antibiotics from wastewater streams, preventing antibiotic exposure to soil and water.

2. Materials and methods

2.1. Materials

All reagents used in biochar characterization and adsorption experiments were of reagent grade and used as received without further purification or modification. SMX and SPY were acquired from TCI Chemicals (Tokyo, Japan) and TMP was acquired from MP Biomedicals (Solon, OH, United States). Solutions were made using deionized ultrapure water (18.2 MΩ cm). Physicochemical properties of TMP, SMX and SPY are shown in the supplementary information (Table S1).

2.2. Biochar production

Date palm leaflets were collected along with fresh fronds grown near Thermal, California. Leaflets were removed and then placed in an oven and heated at 60 °C until dried. After drying, leaflets were cut into roughly 1 cm pieces prior to pyrolysis. Pistachio shells were acquired commercially. Biochars were produced in a Carbolite Gero TF1–1200 furnace (Carbolite Gero, Hope, UK). Samples were heated under N_2 flow (1 L min^{-1}) from ambient temperature to 400, 600 or 800 °C at a rate of 5 °C min^{-1}. Samples were then pyrolyzed at respective target temperatures for 3 h and cooled to room temperature. After pyrolysis, biochars were hand ground and sieved to 80 mesh (180 μm) prior to further use.

2.3. Biochar characterization

The specific surface area of the biochar was determined by a single-point BET N_2 adsorption isotherm. N_2 adsorption was measured on a Quantasorb Jr. surface area analyzer (Quantachrome Corp., Syosset, NY). Biochar moisture, ash, volatile and fixed carbon contents were determined by ASTM method D1762-84 (ASTM, 2013). C and N concentrations were determined through combustion analysis and O and H concentrations were determined through pyrolysis on a Elementar Vario PYRO Cube (Elementar Americas Inc., Ronkonkoma, NY). Attenuated total reflectance–Fourier transform infrared (ATR–FTIR) spectra of the biochars were collected on a Bruker Invenio-R spectrometer (Bruker Optics Inc., Billerica, MA). Cation exchange capacity (CEC) was determined by the modified ammonium acetate compulsory displacement method (Lago et al., 2021). Zeta potentials were determined by microelectrophoresis with a Zeta-Meter 3.0 instrument (Zeta Meter, Long Island City, NY). Further methodological details on ATR-FTIR spectroscopy and CEC determination may be found in the supplementary information.

2.4. Adsorption experiments

Equilibrium adsorption of antibiotics in a ternary antibiotic mixture was studied using two different methodologies: (i) determination of a partitioning coefficient (K_d) and removal efficiency at a fixed environmentally relevant concentration of 10 μg L^{-1} for each antibiotic and (ii) assessment of equilibrium adsorption isotherms across a wider range of concentrations (5 to 100 mg L^{-1}). For K_d and removal efficiency determination, 0.2 g of each biochar was added to 10 mL of aqueous solution containing 10 μg L^{-1} of SMX, SPY and TMP. These studies were conducted in glass vials with Teflon-coated septa. For adsorption isotherm studies, the same solution volume and solid concentration were used as in partitioning coefficient studies. Initial SMX, SPY and TMP concentrations of 5, 10, 20, 30, 40, 60 and 100 mg L^{-1} were used. Suspensions were then shaken in a dark room for 24 h. A period of 24 h was found to be adequate to reach equilibrium in previous studies

probing adsorption of SMX, SPY and TMP onto biochars (Huang et al., 2020; Stylianou et al., 2021). Equilibrium solution samples were then withdrawn from vials, centrifuged at 14,000 rpm, and the supernatant passed through a 0.2 μm PTFE syringe filter into an amber glass vial before liquid chromatography–tandem mass spectrometric (LC–MS/MS) analysis. Adsorption was quantified as the difference between initial and final amounts of SMX, SPY and TMP in solution. All adsorption studies were performed in triplicate ($n = 3$). In adsorption studies, suspensions were not pH adjusted and matched the inherent pH of biochars.

Adsorption isotherms were fitted by the Langmuir model, described as:

$$q_e = \frac{q_{max} K c_{eq}}{1 + K c_{eq}}$$

where q_e is the amount of antibiotic adsorbed (mg g^{-1}) at equilibrium concentration c_{eq} (mg L^{-1}), q_{max} is the maximum adsorption capacity (mg g^{-1}) and K is the Langmuir adsorption coefficient (L mg^{-1}) (McBride, 1994). It should be noted that despite the description of adsorption behavior, no robust inferences regarding adsorption mechanisms can be inferred from adherence to the Langmuir model itself. Several assumptions (e.g., energetically homogeneous surface sites, monolayer adsorption on sites, no interaction amongst adsorbed species) are violated in the biochar-solution system. Inferences regarding adsorption energetics and adsorbate orientation are consequently not physically meaningful (Essington, 2004). The model, however, is still suited for describing empirical adsorption curve characteristics and equilibrium partitioning behavior in systems where the underlying model assumptions do not apply (Essington, 2004).

For partitioning coefficient studies, K_d values were determined by:

$$K_d = \frac{c_s}{c_{aq}}$$

where K_d is the partitioning coefficient (L kg^{-1}), c_s is the antibiotic concentration in solid phase (μg kg^{-1}) and c_{aq} is the aqueous phase concentration (μg L^{-1}) (McBride, 1994).

Removal efficiencies were calculated by:

$$RE = \left(\frac{c_0 - c_e}{c_0}\right) * 100$$

where RE is the removal efficiency (%), c_0 is the initial concentration of antibiotics in solution (μg L^{-1}) and c_e is the concentration in solution after adsorption equilibrium (μg L^{-1}).

2.5. LC–MS/MS analysis

LC–MS/MS analyses were performed on an Agilent 1290 Infinity II HPLC with an Agilent 6410B triple quadrupole MS/MS detector and an electrospray ionization interface. Additional information regarding LC-MS/MS methods may be found in the supplementary information.

3. Results and discussion

3.1. Biochar specific surface area

PS biochars had surface areas ranging from 3.89 to 66.85 $m^2\ g^{-1}$ and DPL biochars ranged from 5.75 to 70.38 $m^2\ g^{-1}$ (Table 1). This is attributable to the thermal transformation of feedstocks during pyrolysis, which liberates volatile matter and thermally decomposes functionalities present in feedstocks, producing high surface area pore structures in biochar (Tomczyk et al., 2020). The observed ranges of surface areas are generally consistent with previously reported values for PS and DPL biochars (196.4 and ≈3.5–289 $m^2\ g^{-1}$, respectively), albeit somewhat lower (Komnitsas and Zaharaki, 2016; Sizirici et al., 2021). Observed surface area values were higher for PS biochars than DPL biochar produced at 400 °C. At 600 and 800 °C, DPL yielded biochars with higher surface area than did PS. These results suggest there was no clear relationship between feedstock and surface area. A more pronounced relationship is apparent when comparing biochars produced at different temperatures. For both feedstocks, biochar surface areas generally increased with increasing pyrolysis temperature. An exception to this trend is the pistachio shell biochar produced at 600 °C, which had a slightly lower surface area than pistachio shell biochar produced at 400 °C. These findings are in agreement with several previous studies, which report an increase in surface area with increasing pyrolysis temperature due to enhanced release of volatile matter and increase in micropore volume (Keiluweit et al., 2010; Ndoun et al., 2021).

3.2. Proximate analysis of biochars

Volatile, fixed C and ash contents varied considerably between biochars (Table 1). DPL biochars had a higher range of ash contents (17.8–25.46 %) relative to PS biochars (1.34–2.55 %). This difference was largely compensated for by a greater proportion of fixed C in PS biochars (74.30–89.69 %) relative to DPL biochars (56.56–65.31 %). The higher ash content in date palm leaves was possibly due to a relatively higher concentration of inorganic elements (e.g., Ca, K, Si, Fe) in date palm leaves compared with pistachio shells, which may translate to a greater proportion of ash-related materials (e.g., quartz, amorphous SiO_2, carbonates) in biochars (Cao and Harris, 2010). Unlike fixed C and ash contents, volatile contents were similar between biochars produced from both feedstocks at a given pyrolysis temperature. Across pyrolysis temperatures, there was a notable effect on the volatile, fixed C and ash contents of the biochars. For the DPL biochars, increasing pyrolysis temperature reduced the proportion of volatile matter and resulted in a relative enrichment of fixed C and ash species. A similar loss of volatiles occurred for PS feedstock biochars, although only a relative enrichment of fixed C was observed. Relative enrichment of thermally recalcitrant fixed C and ash species with increasing pyrolysis temperatures, as observed here, is commonly reported in the literature (Tomczyk et al., 2020).

Table 1
Surface areas, elemental concentrations (C, N, O and H), elemental atomic ratios and volatile, fixed C and ash percentages for biochars produced from DPL and PS feedstocks from 400 to 800 °C. Volatile, fixed C and ash contents represent percentages of moisture-free biochar masses. Elemental concentrations and ratios represent averages of three replicates.

Biochar	Surface area ($m^2\ g^{-1}$)	%C	%N	%O	%H	H/C	O/C	(O + N)/C	% volatile	% fixed C	% ash
DPL 400	5.75	61.55	2.06	13.37	3.45	0.65	0.19	0.22	25.64	56.56	17.80
DPL 600	18.72	64.13	1.95	4.67	2.20	0.32	0.13	0.16	11.45	65.31	23.24
DPL 800	70.38	65.48	1.90	4.12	0.91	0.18	0.12	0.15	9.41	65.13	25.46
PS 400	8.53	74.83	0.35	15.50	3.36	0.55	0.13	0.14	23.46	74.30	2.23
PS 600	3.89	88.55	0.32	11.20	1.74	0.29	0.039	0.043	8.97	89.69	1.34
PS 800	66.85	87.18	0.73	10.54	1.01	0.12	0.036	0.043	9.62	87.83	2.55

3.3. Elemental composition of biochars

C, N, O and H concentrations and related atomic ratios of biochars are shown in Table 1. PS feedstock yielded biochar with a greater proportion of C and O than the DPL feedstock at each pyrolysis temperature. N concentrations, however, were higher in the DPL biochars. H concentrations between chars from both feedstocks were similar for each temperature. Variation in C, N, O and H concentrations between biochars from both feedstocks translated to differences in functional indices related to biochar aromaticity (H/C ratio), hydrophobicity (O/C ratio) and polarity ((O + N)/C ratio) (Zhao et al., 2019). Biochar H/C and O/C ratios are inversely proportional to aromaticity and hydrophobicity, respectively, with the (O + N)/C ratio proportional to biochar polarity. The higher H/C as well as O/C and (O + N)/C ratios of DPL biochars indicate a lower degree of aromaticity and hydrophobicity relative to PS biochars at corresponding pyrolysis temperatures. Pyrolysis temperature had a comparatively greater influence on biochar elemental composition than did feedstock. For a given feedstock, increasing pyrolysis temperature increased C content and decreased concentrations of O and H. Reduction of O and H concentrations with increasing pyrolysis is widely reported in the literature and is attributable to loss or modification of thermally labile functional groups. This includes the loss of hydroxyl (—OH), carboxyl (—COOH), cellulose-like O-alkyl (C—O) and aliphatic (—CH_2—) groups along with the condensation of aromatic structures into conjugated graphitic domains (Ippolito et al., 2020; Keiluweit et al., 2010; Novak et al., 2009; Sun et al., 2018; Tomczyk et al., 2020). Accordingly, pyrolysis-induced shifts in functional group composition create biochars that are more aromatic, more hydrophobic and less polar when pyrolyzed at higher temperatures. The H/C, O/C and (O + N)/C ratios of biochars in this study reflect this, with biochars from both feedstocks having lower values for all ratios as pyrolysis temperature increased.

3.4. Biochar functional group speciation

ATR–FTIR spectra of DPL and PS biochars show the presence of distinct organic functional groups in produced biochar matrices (Fig. S1). Prominent functional group vibrations include ν O—H (≈3350 cm^{-1}), ν_{as} —CH_2 (≈2920 cm^{-1}), ν_s —CH_2 (≈2850 cm^{-1}) ν C═O (≈1690 cm^{-1}), ν C═C (≈1585 cm^{-1}), aromatic ν C—O (≈1370 and 1220 cm^{-1}), aliphatic δ C—H (≈1430 cm^{-1}), ν C—O (≈1100 cm^{-1}) and aromatic δ C—H (≈870, 800 and 750 cm^{-1}) modes (Keiluweit et al., 2010; Parikh et al., 2014). The presence of these functional groups in biochars reflects the largely lignin, cellulose and hemicellulose-rich nutshell and leaf feedstocks used here through thermal recalcitrance and/or thermal modification of these groups. Furthermore, the prominent feature ≈1100 cm^{-1} may also overlap with ash-related ν Si—O and ν Al—O vibrational modes (Parikh et al., 2014). DPL and PS biochars showed some differences, including a more pronounced peak near 1100 cm^{-1} and a weaker feature attributable to aromatic ν C—O near 1220 cm^{-1} in DPL biochars relative to PS biochars. A possible explanation for the more pronounced peak near 1100 cm^{-1} is the greater ash content of DPL chars. ATR–FTIR spectra of ash collected from ash determination showed several features in proximity to this peak, indicating that ash may contribute to this peak's prominence (Fig. S2). The greater ash content may also obscure the aromatic ν C—O stretching mode at around 1220 cm^{-1}, reducing it to a shoulder in spectra of DPL biochars. As with the aforementioned biochar characteristics, pyrolysis temperature had a comparatively large impact on biochar functional group composition relative to feedstock. With increasing pyrolysis temperature across the 400–800 °C temperature range used in this study, a decrease in functional group diversity was observed. Compared with biochar spectra at 400 °C, ν O—H, ν_{as} —CH_2, ν_s —CH_2, ν C═O, aromatic ν C—O and aliphatic/aromatic δ C—H modes are largely diminished or absent in 800 °C biochar spectra. For the features related to O—H, C═O and aliphatic C—H functional groups, the greatest decrease occurred between 400 and 600 °C, likely due to thermal breakdown of lignin and cellulose-like components of biochars which contain these functional groups. Aromatic C—O and C—H functionalities underwent more pronounced removal from 600 to 800 °C, suggesting a greater degree of thermal stability for these aromatic-associated functional groups relative to O—H C═O and aliphatic C—H moieties. Loss of these aromatic associated functional groups indicated condensation into extended structures, through which aromatic C bonds to —H or other functional groups (e.g., COOH, COH) are replaced with bonds to other aromatic C rings. Formed condensed aromatic structures are highly nonpolar and therefore do not efficiently absorb infrared radiation (Parikh et al., 2014). As a result, spectra of 800 °C biochars do not show many prominent features except for the ash related peak near 1100 cm^{-1} in the DPL 800 spectrum. A previous FTIR and X-ray absorption near edge structure study described similar transformation of wood and grass biochars (Keiluweit et al., 2010). A loss of hydroxyl groups was observed at pyrolysis temperatures up to 300 °C, followed by transformation of lignin and cellulose at around 400 °C and extensive condensation of aromatic groups starting at 500 °C and increasing with temperature (Keiluweit et al., 2010).

3.5. Biochar pH, CEC and surface charge

The differing mass fractions, elemental compositions and functional group speciation of biochars resulted in materials with distinct pH, CEC, and zeta potential values (Table 2). The pH values of all biochars were basic, ranging from pH 7.89 to 10.15. DPL biochars generally had higher pH values than did PS biochars, likely due to the higher ash content of DPL biochars which may include (hydr)oxides and carbonates of Na, K, Mg and Ca (Cao and Harris, 2010). With increasing pyrolysis temperature, the pH of the biochars also increased. For the DPL biochars, this is potentially attributable to an increase in ash content with pyrolysis temperature. For PS biochars with ash contents varying little with pyrolysis temperature, the increased pH value might correspond with thermal decomposition of acidic functional groups (e.g., carboxylic and phenolic functionalities) (Novak et al., 2009). ATR–FTIR results suggest this may be a contributing factor, as extensive removal of these groups occurred, particularly from 400 to 600 °C where the largest increase in pH values was observed.

All produced biochars had negative zeta potential values in solutions with unbuffered pH. Zeta potential values of DPL biochars were consistently lower than for PS biochars, indicating a greater negative surface charge on DPL biochar surfaces relative to PS biochars. As with pH, this was potentially related to an overall higher ash content in DPL biochars. Many mineral species present in biochar ash (e.g., silicon oxide, carbonate minerals) have point of zero charges that are well below the unbuffered pH values of biochars in this study. For example, Si-oxides commonly have point of zero charge values ≈2.0–3.0 with Al-oxides closer to ≈8.0–9.0 (Essington, 2004). There was no straightforward relationship between pyrolysis temperature and zeta potential despite the link between the two parameters.

CEC values were somewhat higher for DPL biochars compared with PS biochars. Pyrolysis temperature did not have a systematic impact on

Table 2
Biochar characteristics functionally associated with surface charge, pH and cation exchange behavior. CEC (n = 2) and pH (n = 3) values represent an average of experimental replicates and zeta potential represents an average of readings from at least 20 particles.

Biochar	pH	Zeta potential (mV)	CEC ($cmol_c\ kg^{-1}$)
DPL 400	9.09	−44.1	18.26
DPL 600	10.04	−37.65	8.24
DPL 800	10.15	−39.04	8.40
PS 400	7.89	−22.35	7.78
PS 600	9.19	−25.57	6.32
PS 800	9.39	−27.81	7.13

CEC, although DPL biochars showed a decrease in CEC above 400 °C. A recent meta-analysis found a similar lack of relationship between pyrolysis temperature and CEC (Ippolito et al., 2020). This observation largely reflected trends in biochar zeta potentials here, which were lower for DPL biochars and showed only a nominal influence of pyrolysis temperature. Given the relationship between negative surface charge and the capacity of a particle to adsorb cations, the similarity in behavior between these two parameters is physically consistent.

3.6. Antibiotic adsorption isotherms and relation to biochar properties

All antibiotics readily adsorbed onto all produced biochars from ternary mixtures ranging from 5 to 100 mg L^{-1} initial concentration (Fig. 1, Table 3). Across this range, adsorption behavior was well fit by the Langmuir model, although the observed adsorption isotherm characteristics differed amongst biochars and antibiotics. Of particular relevance to the performance of biochars for antibiotic removal is the Langmuir q_{max} parameter, which provides an empirical estimate of biochar adsorption capacity for antibiotics. Maximum predicted adsorption capacity ranges for TMP (0.91–4.01 mg g^{-1}), SMX (0.29–3.61) and SPY (0.59–166 mg g^{-1}) varied considerably between biochars, but were generally in agreement with the range of adsorption capacities reported in the literature (TMP: 2.08–125.88 mg g^{-1}; SMX: 0.25–128.2 mg g^{-1}; SPY: 0.013–57.9 mg g^{-1}) (Berges et al., 2021; Huang et al., 2020; Li et al., 2019; Ndoun et al., 2021; Sun et al., 2016). Our predicted capacities are on the lower end of reported values (except for SPY on DPL 400 biochar), possibly due to the presence of three antibiotics in solution that may simultaneously adsorb on available surface sites rather than a single species. Total predicted antibiotic adsorption capacities of biochars ranged from 1.26 to 173 mg g^{-1} for PS 800 and DPL 400 biochars, respectively. These values compare more closely with the reported values for individual antibiotics and indicate some degree of competition might influence adsorption capacity with the antibiotic mixture used here. Differences in biochar physicochemical properties, however, make this comparison tentative.

Adsorption capacities were typically higher for DPL biochars at a given pyrolysis temperature compared with PS biochars. Increasing pyrolysis temperature generally decreased adsorption capacity, with the largest decrease observed from 400 to 600 °C. To help understand variation in adsorption capacity in relation to underlying biochar properties, correlation analysis was conducted (Fig. 2). For all three antibiotics, the strongest correlation for q_{max} is with CEC, with TMP, SMX and SPY having correlation coefficients of 0.98, 0.98 and 0.99, respectively. The net negative (SMX and SPY) or neutral (TMP) charges on antibiotics across the biochar pH range of 7.89–10.15 made the relationship with CEC (which is a measure of negatively charged cation exchange sites) unexpected, as electrostatic interactions with negatively charged sites would not be favorable. CEC is a functional metric of cation exchange dependent upon several factors, including pH, surface functional groups and elemental composition. It is unlikely that negative charge itself contributed to the adsorption capacity of these antibiotics, but perhaps the density of biochar surface functional groups that lead to surface charge development (e.g., carboxylate and phenol groups) influenced antibiotic adsorption capacity. This would correspond with the decrease in polar functional groups (from ATR–FTIR spectra) with increasing pyrolysis temperature and the coinciding decrease in q_{max}. Furthermore, O/C and (O + N)/C ratios correlated reasonably well with observed adsorption capacities. Both points indicate that O-containing

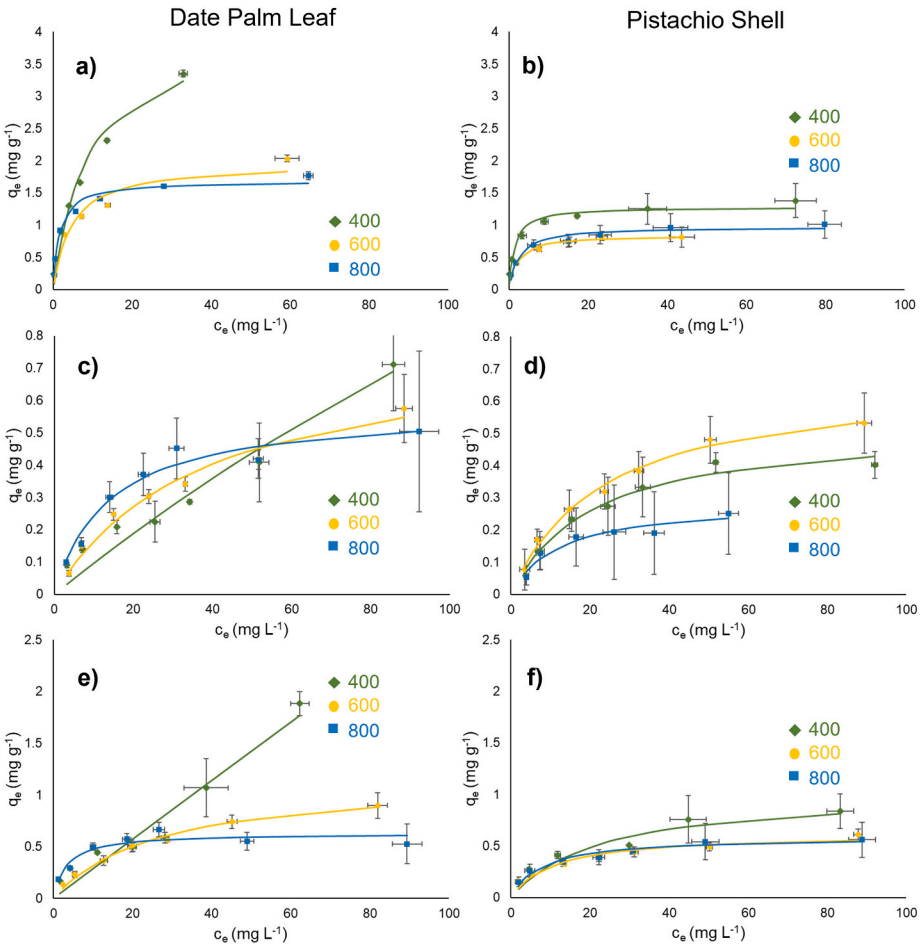

Fig. 1. Averaged experimental adsorption isotherms (points) and Langmuir model fitting (solid lines) for trimethoprim (a, b), sulfamethoxazole (c, d) and sulfapyridine (e, f). Different pyrolysis temperatures are denoted by different shaped points (400 °C – diamonds, 600 °C – circles, 800 °C-squares) and corresponding colors (400 °C – green, 600 °C – yellow, 800 °C-blue). Error bars represent standard deviation ($n = 3$) of c_e and q_e. (For interpretation of the references to color in this figure legend, the reader is referred to the web version of this article.)

Table 3
Langmuir model parameters from averaged isotherms for each antibiotic and biochar sample.

Biochar	Trimethoprim			Sulfamethoxazole			Sulfapyridine			Total
	K (L mg^{-1})	q_{max} (mg g^{-1})	RMSE	K (L mg^{-1})	q_{max} (mg g^{-1})	RMSE	K (L mg^{-1})	q_{max} (mg g^{-1})	RMSE	q_{max} (mg g^{-1})
DPL 400	1.13×10^{-1}	4.10	1.52×10^{-1}	2.75×10^{-3}	3.61	4.58×10^{-2}	1.73×10^{-4}	1.66×10^{2}	1.36×10^{-1}	1.73×10^{2}
DPL 600	2.16×10^{-1}	1.98	1.48×10^{-1}	2.66×10^{-2}	7.81×10^{-1}	2.28×10^{-2}	3.69×10^{-2}	1.18	2.81×10^{-2}	3.94
DPL 800	6.25×10^{-1}	1.69	8.17×10^{-2}	7.22×10^{-2}	5.81×10^{-1}	2.90×10^{-2}	3.08×10^{-1}	6.28×10^{-1}	5.90×10^{-2}	2.27
PS 400	7.76×10^{-1}	1.28	8.55×10^{-2}	4.92×10^{-2}	5.23×10^{-1}	1.97×10^{-2}	4.46×10^{-2}	1.03	8.08×10^{-2}	2.83
PS 600	5.14×10^{-1}	8.49×10^{-1}	3.58×10^{-2}	4.24×10^{-2}	6.77×10^{-1}	1.41×10^{-2}	9.40×10^{-2}	6.23×10^{-1}	4.09×10^{-2}	1.53
PS 800	4.40×10^{-1}	9.71×10^{-1}	5.53×10^{-2}	8.52×10^{-2}	2.86×10^{-1}	1.66×10^{-2}	1.31×10^{-1}	5.87×10^{-1}	3.24×10^{-2}	1.26

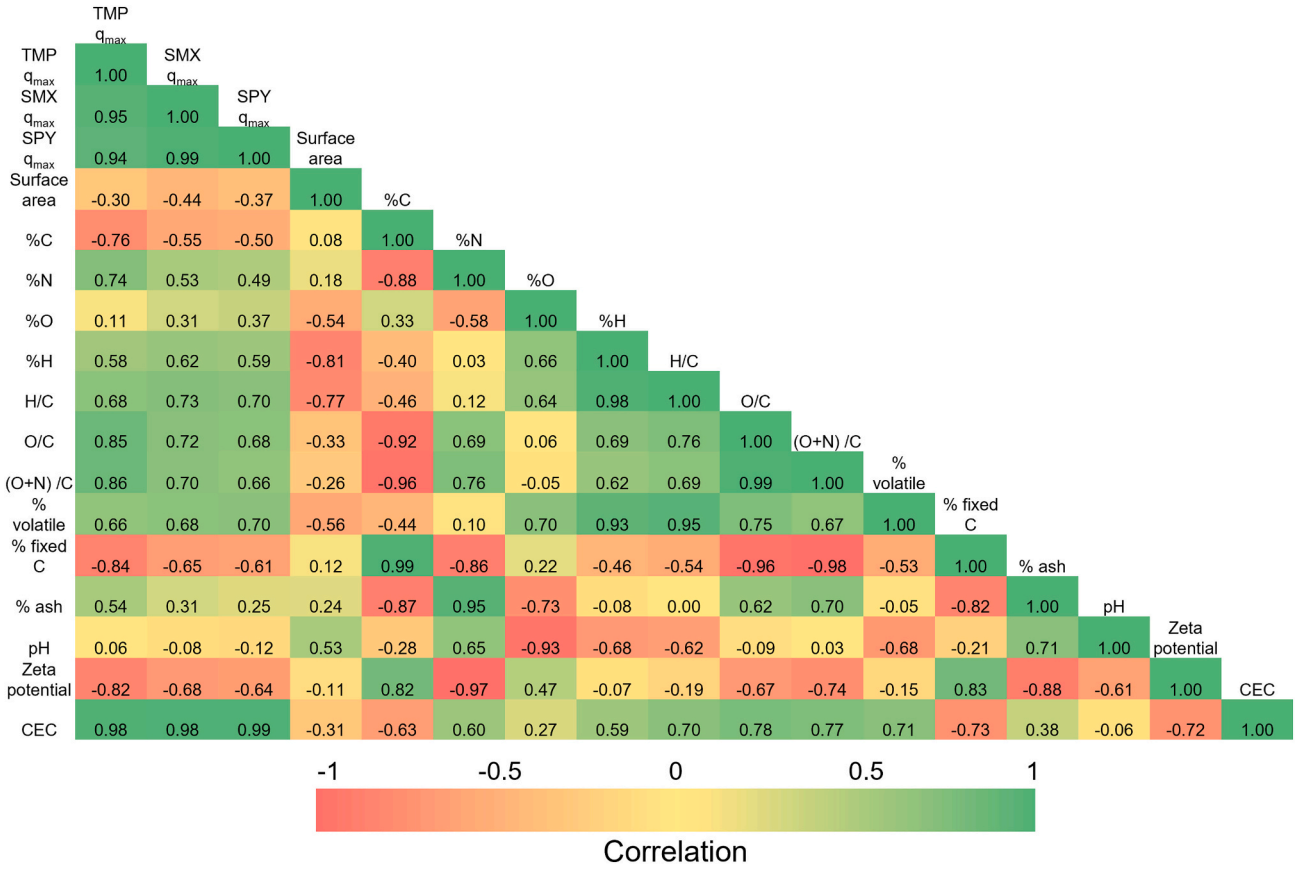

Fig. 2. Correlation matrix between predicted adsorption capacity (q_{max}) and biochar physicochemical characteristics.

functional groups played a key role in adsorbing these antibiotics under studied conditions. C—O/C═O containing surface functionalities have also been previously identified for predicting pharmaceutical adsorption on biochars, providing additional evidence for the role of these groups within CEC-related influence (Zhu et al., 2022).

Through these relationships, some insights into the antibiotic adsorption mechanisms onto biochar may be inferred. For neutral TMP, adsorption onto polar functional groups could have included H-bonding through amino, methoxy and pyrimidine groups. Carboxylic functional groups on biochar may also enhance π electron withdrawal from aromatic structures on biochar, rendering π electron deficient aromatic structures that could serve as sites for π electron donation by the pyrimidine structure of TMP through π-π electron donor-acceptor (EDA) interactions (Liu et al., 2015). For negatively charged SMX and SPY at high corresponding biochar pH values, these surface sites might have aided in the formation of charge assisted H-bonds. This process involves the exchange of a proton from H_2O to a negatively charged ion, forming an OH^- and neutrally charged compound that can readily form H-bonds with O-containing surface functional groups (Teixidó et al., 2011). Negatively charged sulfonamide groups in SPY and SMX could conceivably form neutral species and engage in H-bonding with polar N or O-containing functional groups. An increase in surface adsorption capacity beyond adsorption attributable to π-π interactions would then become accessible. Charge assisted H-bonding of SPY and SMX would be consistent with other studies that showed appreciable adsorption of negatively charged sulfonamides onto negatively charged biochar surfaces (Ndoun et al., 2021; Teixidó et al., 2011; Zheng et al., 2013). These findings were consistent with our characterization results, which showed a decrease in O-containing functional groups as well as CEC, (O + N/C) and O/C with increasing pyrolysis temperature. As with biochar adsorption capacity, the most pronounced changes to these characteristics occurred from 400 to 600 °C. The comparatively higher adsorption capacities for DPL biochars versus PS biochars also related well to the physicochemical characteristics of biochars from different feedstocks. Namely, the greater CEC, (O + N/C) and O/C values for DPL biochars compared to PS biochars corresponded with the greater adsorption capacities of these chars across the 400–800 °C pyrolysis temperature range.

Langmuir K values determined for each antibiotic and biochar showed highest values for TMP, followed by SPY, which generally had

higher affinities than SMX (Table 3). This was likely attributable to the net charges on TMP, SMX and SPY molecules at biochar pH values. The negative charges on SMX and SPY likely led to a lower affinity with negatively charged biochar surfaces relative to charge neutral TMP due to repulsive electrostatic interaction, which can greatly reduce adsorption affinity. Between feedstocks, PS biochars generally showed greater adsorption affinities when compared to DPL biochars at a given pyrolysis temperature. Electrostatic repulsion also played a probable role in the lower general affinity of SMX and SPY for DPL biochars, as these biochars possessed a more negative charge than did PS biochars. Pyrolysis temperature had a greater influence on K values than did feedstock for all antibiotics, with K and pyrolysis temperature increasing concertedly. The exception to this was adsorption affinity of TMP on PS biochars, which decreased somewhat with increasing pyrolysis temperature. Increasing adsorption affinity with higher biochar pyrolysis temperatures is a trend previously observed for the adsorption of organic compounds onto biochar, including sulfonamide antibiotics (Zheng et al., 2013). This relationship was attributed to decreasing biochar polarity/increasing hydrophobicity with pyrolysis temperature observed here for both DPL and PS biochars, which reduces the affinity of water for biochar surfaces by reducing the size and density of water clusters around polar functional groups, enhancing favorability of hydrophobic interaction (Wang et al., 2006). This indicated that hydrophobic interaction, such as π-π interactions, played a role in antibiotic adsorption onto biochar in addition to the aforementioned H-bonding and EDA processes. These hydrophobic forces likely became more prevalent on condensed, hydrophobic biochar surfaces produced at higher pyrolysis temperature.

3.7. Biochar antibiotic removal performance at trace concentrations

K_d values for TMP, SMX and SPY on all biochars are shown in Fig. 3 (see also supplementary information (Table S2)). K_d values differed between antibiotic species, with K_d ranging from 1012.08 to 2029.15 L mg^{-1} for TMP, 15.87 to 2690.56 mL g^{-1} for SMX and 168.28 to 9347.8 mL g^{-1} for SPY. Across both feedstocks and all pyrolysis temperatures, K_d values for TMP were lower for PS biochars and showed a decreasing trend with increasing pyrolysis temperature, albeit not significantly. SMX distribution coefficients increased significantly with pyrolysis temperature for both feedstocks, with PS biochar showing greater affinity than DPL at 600 °C and DPL showing a greater affinity than PS at 800 °C. SPY exhibited similar behavior, with DPL biochars showing progressively greater K_d values from 400 to 600 °C and from 600 to 800 °C. PS biochars had greater K_d values at higher pyrolysis temperatures relative to 400 °C, while no significant difference was observed between 600 and 800 °C. At 400 and 600 °C, DPL biochars had significantly lower K_d values relative to PS biochars, and both were similar at 800 °C.

Correlation analysis between K_d and biochar physicochemical characteristics linked these adsorption characteristics with biochar properties (Fig. 4). Unlike correlations with biochar adsorption capacity, CEC was not the strongest correlating feature with antibiotic K_d values. There were some similarities, however, with elemental composition correlating strongly to partitioning behavior for all antibiotics, with surface

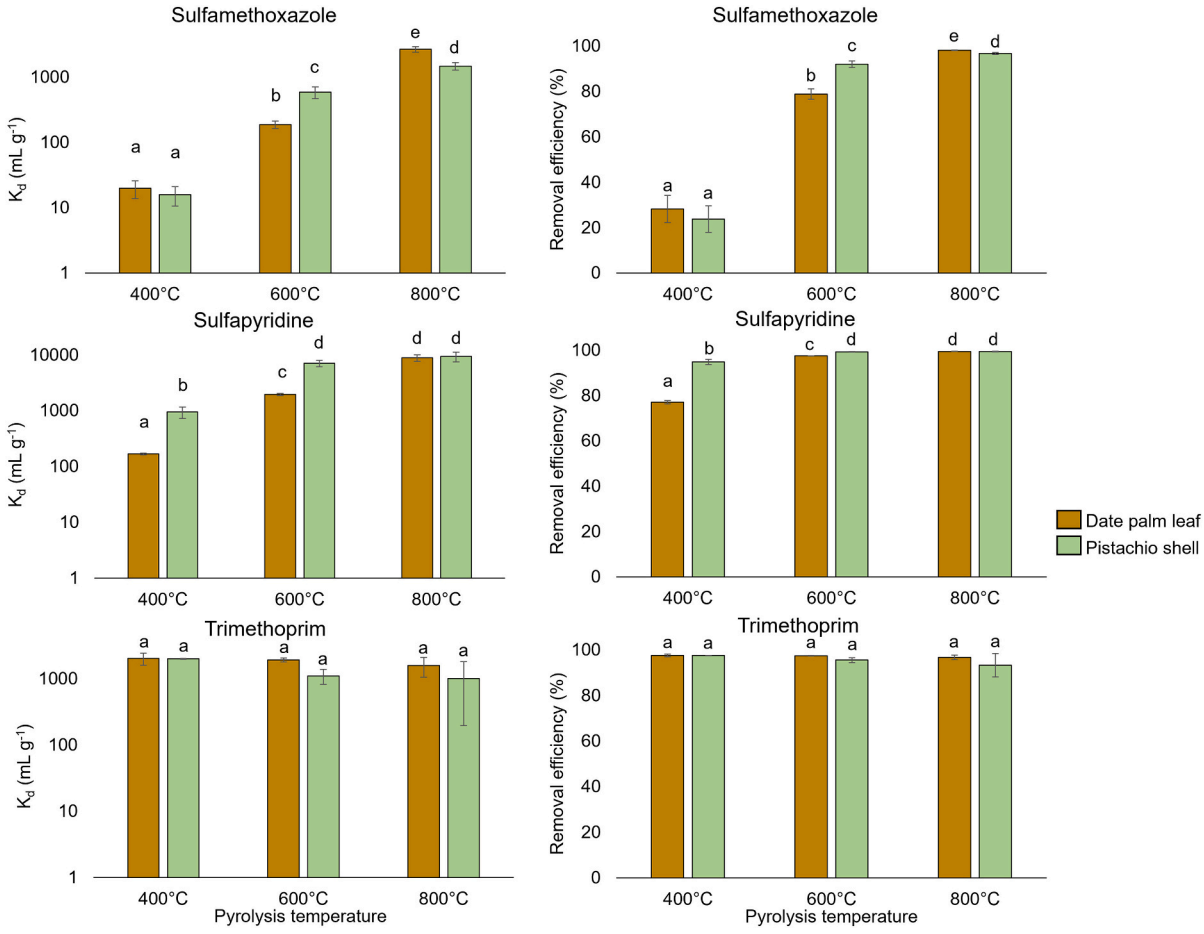

Fig. 3. Experimental distribution coefficients for DPL (brown bars) and PS (green bars) biochars at 400, 600 and 800 °C determined in a 10 ppb (μg L^{-1}) solution of each antibiotic (left). Experimental removal efficiencies for DPL and PS biochars at 400, 600 and 800 °C determined in a 10 μg L^{-1} solution of each antibiotic (right). Error bars represent standard deviations ($n = 3$) and letters indicate significant ($p < 0.05$) differences between groups for each antibiotic based on Student's *t*-test. K_d values are presented on a log scale. (For interpretation of the references to color in this figure legend, the reader is referred to the web version of this article.)

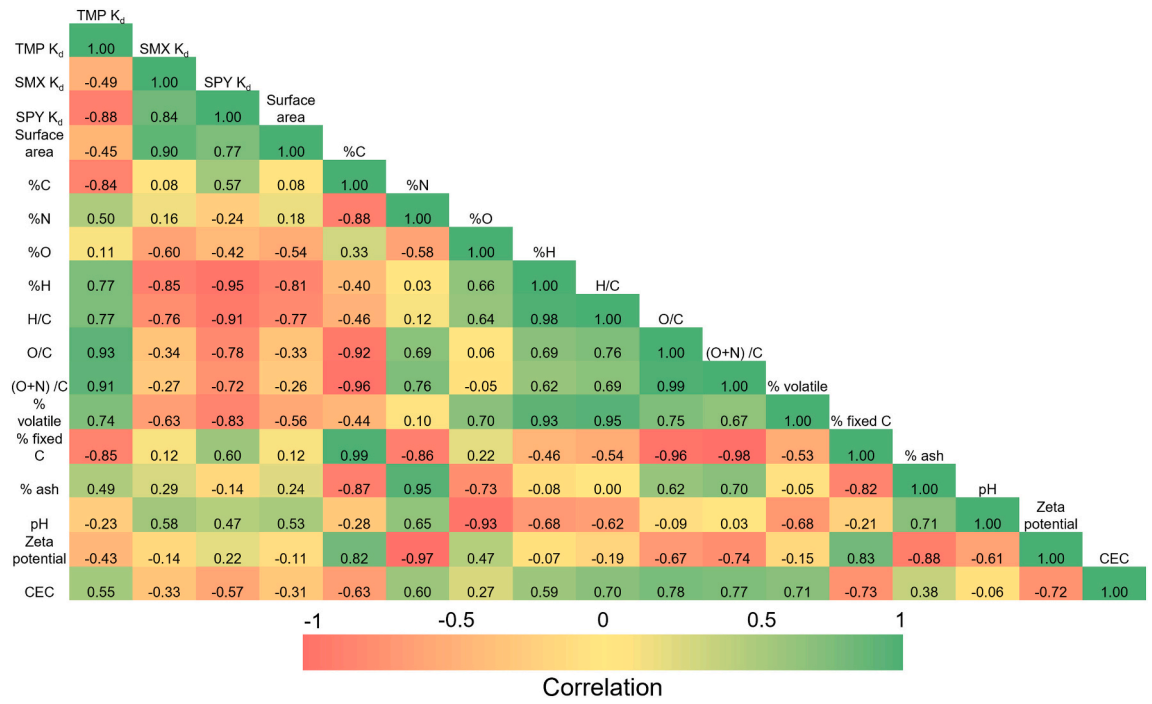

Fig. 4. Correlation matrix between predicted antibiotic distribution coefficients (K_d) and biochar physicochemical characteristics.

area also correlating well to K_d for SMX and SPY. More specifically, SMX and SPY had strong negative correlations with %H and H/C ratio. While these characteristics covaried strongly, they collectively indicated a trend of increasing K_d with increasing biochar hydrophobicity. Similar to the Langmuir coefficient derived from a much higher concentration range, this implied that high-affinity π-π interactions occur between SMX/SPY and biochar surfaces. This would lead to stronger partitioning onto more hydrophobic biochars relative to charge assisted H-bonding that potentially occurred, as well on more polar biochar surface sites. Given the relationship between increasing pyrolysis temperature and increasing biochar hydrophobicity through the formation of graphitic domains, the observed differences in SMX and SPY K_d values between biochars pyrolyzed at different temperatures were likely attributable to these hydrophobic interactions (Tomczyk et al., 2020; Zheng et al., 2013). ATR–FTIR spectra also reflected the transition from biochars relatively enriched in polar functional groups at 400 °C and transitioning to largely ash and condensed aromatic structures at higher temperatures. This potentially linked to feedstock effects as well, as PS biochars generally had lower H/C ratios than did DPL biochars, albeit slightly. Although TMP K_d values did not vary significantly across biochars, there was a strong correlation between K_d values and biochar O/C and (O + N)/C ratios. The presence of polar functional groups could enhance TMP adsorption through providing sites for H-bonding or electronic effects favorable to π-π EDA interactions. Furthermore, it is also conceivable that the presence of these groups reduced hydrophobicity and disproportionately reduced the affinity of SMX and SPY for biochars, effectively reducing surface site competition. Given the similarity of TMP K_d values across all biochars, however, these influences were likely minimal. In addition to these surface functional group influences, SMX and SPY K_d values correlated with biochar surface area. This is consistent with previous findings which showed greater sulfonamide partitioning with higher surface area biochars (Huang et al., 2020; Zheng et al., 2013). This influence was attributed to enhancement of hydrophobic interactions due to increased surface area, which would align with our observed relationship between K_d and surface composition (Huang et al., 2020; Peiris et al., 2017).

As partitioning behavior and removal efficiency are related parameters, observed trends in K_d for biochars and antibiotics translated to a range of removal efficiencies between antibiotics and biochars (Fig. 3 and see supplementary information (Table S2)). Biochars showed the most consistent and thorough removal of TMP from solution, with removal efficiencies ranging from 93.33 to 97.58 %. SMX and SPY removal were more dependent on biochar properties, with removal efficiencies ranging from 23.78 to 98.1 % and 77.08 to 99.45 %, respectively. Across PS and DPL feedstocks at different pyrolysis temperatures, TMP removal efficiency did not vary significantly. SPY showed more variability, with DPL biochars progressively removing more SPY from solution with incremental pyrolysis temperature increases. PS biochars removed more SPY from solution at 600 and 800 °C relative to 400 °C, with no difference between the higher pyrolysis temperatures. At 400 and 600 °C, PS biochars removed significantly more SPY from solution than did DPL biochars. Similar to SPY, SMX removal showed variation between feedstocks and pyrolysis temperatures. For 600 °C biochars, PS feedstock resulted in more effective removal, whereas at 800 °C DPL biochar was more effective than was 800 °C PS biochar. For a given feedstock, increasing pyrolysis temperature led to greater SMX removal efficiencies. Considering the direct relationship between K_d and removal efficiency, the same biochar characteristics governed removal efficiencies. Most marked was the influence of feedstock and pyrolysis temperature on biochar hydrophobicity, which drove significant differences in SMX and SPY adsorption through hydrophobic interaction.

DPL and PS biochars showed great potential for the removal of TMP, SMX and SPY from solution at an environmentally relevant concentration. Comparison with previous studies is complicated by differences in experimental concentrations, which often well exceed environmental relevance for methodological purposes, and biochar loading rates. Some general comparisons, however, show that DPL and PS biochars produced in this study demonstrated strong removal characteristics. For example, a recent study by Stylianou et al. demonstrated poor removal of SMX by biosolids, manure and coffee ground biochar (up to 10–20 %) from a mixture of seven antibiotics at 100 μg L^{-1} concentration with both 1 and 10 g L^{-1} biochar concentrations (Stylianou et al., 2021). The authors attributed poor removal to the net negative charge on SMX under alkaline pH and adsorptive competition from other solutes. While our study used lower antibiotic concentrations and a higher biochar loading (20 g L^{-1}), we observed almost complete removal (up to 98.1 %) of SMX

with 800 °C biochars, despite alkaline pH and multiple solute antibiotics. Under single solute conditions, another study showed poor SMX removal by ball-milled hickory chip biochar when pH was at or above 7.5, while effective removal occurred at acidic pH values (Huang et al., 2020). SPY removal was similarly favorable when compared to other findings. Huang et al. showed high SPY removal efficiency of around 85 % at pH 3.5, but removal was 40 % at alkaline pH, as used in our study (pH = 8.5). SPY removal efficiencies of around 70 % and 40 % at pH = 10–11 and 7, respectively, were reported with cotton gin waste biochar (Ndoun et al., 2021). The Ndoun et al. and Huang et al. studies used 10 ppm SMX and SPY for removal efficiency determination, which may explain the lower efficiencies compared with our study (77.08–99.45 %). TMP removal rates were more similar to those reported previously than were those for SMX and SPY. TMP removal efficiencies of 80–90 % were observed for manure and coffee ground biochars (Stylianou et al., 2021). In another study, over 90 % of TMP was removed from a wastewater matrix by woodchip biochar after 7 days incubation (Muter et al., 2019). Both values compare well to our observed TMP removal efficiency range of 93.33–97.58 %. These comparisons collectively highlight the viability of PS and DPL biochars for the removal of trace levels of antibiotics from solutions.

3.8. Selection of biochars for TMP, SMX and SPY removal in water treatment

We demonstrated the production of biochars from two different classes of agricultural byproduct feedstock (i.e., leaf and nut shell material) at a range of pyrolysis temperatures. This yielded biochars with a matrix of properties that influenced two key parameters related to adsorbent performance: q_{max} and K_d. Interestingly, the two parameters correlate with conflicting trends in biochar characteristics for studied antibiotics. q_{max} correlates positively with CEC and elemental ratios representing surface polarity for TMP, SMX and SPY, whereas increasing biochar hydrophobicity and aromaticity favor greater K_d values for SMX and SPY, with K_d values for TMP not significantly different regardless of biochar characteristics. For the low concentrations of antibiotics often found in treated wastewater (ng L^{-1} to μg L^{-1} levels) that might be used for irrigation purposes, K_d would be the more practical parameter to optimize as high adsorbent affinity is necessary to effectively remove trace levels of solutes. For either of the feedstocks selected here, that suggests pyrolysis at 800 °C would yield the best performing biochar, as shown by the extensive removal of antibiotics in this study. Despite the relatively low predicted antibiotic q_{max} values for biochars produced at 800 °C, ranging from 0.29 to 1.69 mg g^{-1} for individual antibiotics and 1.26–2.27 mg g^{-1} for TMP, SMX and SPY combined, these materials could still treat a high volume of water in a water polishing capacity. It is also possible to utilize an array of biochars to stagger desired removal characteristics, such as in a layered column system, to optimize antibiotic removal from wastewater streams prior to irrigation (Ashworth and Ibekwe, 2020).

4. Conclusions

This work demonstrated the conversion of two agricultural byproducts endogenous to arid and semi-arid growing systems into a range of biochars with functionally different physicochemical characteristics. These properties were easily tailored through simple modification of pyrolysis temperature and yielded a range of adsorption characteristics toward three antibiotics prevalent in treated wastewater streams. Although TMP, SMX and SPY adsorbed strongly on biochars, biochar properties influenced antibiotic adsorption mechanisms, which had a large impact on adsorption behavior at relatively high (0.5–100 mg L^{-1}) and trace (10 μg L^{-1}) antibiotic concentrations. Produced biochars showed excellent potential to optimize adsorption affinity (K_d) and capacity (q_{max}) for each antibiotic used and, hence, demonstrated comprehensive antibiotic removal under environmentally relevant trace concentrations. As this study identified key biochar characteristics linked with specific aspects of antibiotic adsorption, this work will aid future efforts to predict antibiotic adsorption from easily measurable properties of biochars produced from other feedstocks and production conditions. Lastly, as the DPL and PS feedstocks used here are widely available in arid growing regions, these tailored adsorption capabilities could be viable at farm, local and regional scales for purifying wastewater for irrigation. While this study shows promising application of DPL and PS biochars for effectively removing a mixture of antibiotics from solution, more studies are needed to fully realize their potential for purifying treated wastewater for irrigation purposes on a larger scale. Understanding antibiotic adsorption behavior under a wider range of solution conditions that could influence performance (e.g., presence of dissolved organic matter, varying pH and ionic strength, influence of multivalent cations, wider range of target solutes) in practical application would be critical. Development of a larger scale filtration system utilizing these adsorbents, including batch and fixed bed systems with single or multi-step treatment systems would be necessary before practical application.

CRediT authorship contribution statement

Michael P. Schmidt: Conceptualization, Formal analysis, Methodology, Writing – original draft, Writing – review & editing. **Daniel J. Ashworth:** Conceptualization, Formal analysis, Writing – review & editing. **Nydia Celis:** Methodology, Writing – review & editing. **Abasiofiok Mark Ibekwe:** Project administration, Writing – review & editing.

Declaration of competing interest

The authors declare that they have no known competing financial interests or personal relationships that could have appeared to influence the work reported in this paper.

Data availability

Data will be made available upon reasonable request to the corresponding author.

Acknowledgements

This work was funded as part of an in-house project by the USDA-ARS. Technical support for the antibiotic adsorption studies was provided by Qiaoping Zhang and Layton Chhour. Dr. Robert Krueger of the USDA-ARS National Clonal Germplasm Repository for Citrus and Dates provided date palm biomass. The findings and conclusions in this publication are those of the author(s) and should not be construed to represent any official USDA or U.S. Government determination or policy. Mention of trade names or commercial products in this publication is solely for the purpose of providing specific information and does not imply recommendation or endorsement by the U.S. Department of Agriculture.

Appendix A. Supplementary data

Supplementary data to this article can be found online at https://doi.org/10.1016/j.biteb.2022.101325.

References

Ashworth, D.J., Ibekwe, A.M., 2020. System of multi-layered environmental media for the removal of antibiotics from wastewater. J. Environ. Chem. Eng. 8, 104206 https://doi.org/10.1016/j.jece.2020.104206.

ASTM, 2013. Chemical Analysis of Wood Charcoal.

Berges, J., Moles, S., Ormad, M.P., Mosteo, R., Gómez, J., 2021. Antibiotics removal from aquatic environments: adsorption of enrofloxacin, trimethoprim, sulfadiazine, and

amoxicillin on vegetal powdered activated carbon. Environ. Sci. Pollut. Res. 28, 8442–8452. https://doi.org/10.1007/s11356-020-10972-0.
Cao, X., Harris, W., 2010. Properties of dairy-manure-derived biochar pertinent to its potential use in remediation. Bioresour. Technol. 101, 5222–5228. https://doi.org/10.1016/j.biortech.2010.02.052.
Chao, C.T., Krueger, R.R., 2007. The Date Palm (Phoenix dactylifera L.): overview of biology, uses, and cultivation. Horts 42, 1077–1082. https://doi.org/10.21273/HORTSCI.42.5.1077.
Dreher, M.L., 2012. Pistachio nuts: composition and potential health benefits. Nutr. Rev. 70, 234–240. https://doi.org/10.1111/j.1753-4887.2011.00467.x.
Essington, M.E., 2004. Soil and Water Chemistry: An Integrative Approach. CRC Press, Boca Raton.
Fu, Q., Malchi, T., Carter, L.J., Li, H., Gan, J., Chefetz, B., 2019. Pharmaceutical and personal care products: from wastewater treatment into agro-food systems. Environ. Sci. Technol. 53, 14083–14090. https://doi.org/10.1021/acs.est.9b06206.
Huang, J., Zimmerman, A.R., Chen, H., Gao, B., 2020. Ball milled biochar effectively removes sulfamethoxazole and sulfapyridine antibiotics from water and wastewater. Environ. Pollut. 258, 113809 https://doi.org/10.1016/j.envpol.2019.113809.
Ippolito, J.A., Cui, L., Kammann, C., Wrage-Mönnig, N., Estavillo, J.M., Fuertes-Mendizabal, T., Cayuela, M.L., Sigua, G., Novak, J., Spokas, K., Borchard, N., 2020. Feedstock choice, pyrolysis temperature and type influence biochar characteristics: a comprehensive meta-data analysis review. Biochar 2, 421–438. https://doi.org/10.1007/s42773-020-00067-x.
Jaramillo, M., Restrepo, I., 2017. Wastewater reuse in agriculture: a review about its limitations and benefits. Sustainability 9, 1734. https://doi.org/10.3390/su9101734.
Kampouris, I.D., Klümper, U., Agrawal, S., Orschler, L., Cacace, D., Kunze, S., Berendonk, T.U., 2021. Treated wastewater irrigation promotes the spread of antibiotic resistance into subsoil pore-water. Environ. Int. 146, 106190 https://doi.org/10.1016/j.envint.2020.106190.
Keiluweit, M., Nico, P.S., Johnson, M.G., Kleber, M., 2010. Dynamic molecular structure of plant biomass-derived black carbon (biochar). Environ. Sci. Technol. 44, 1247–1253. https://doi.org/10.1021/es9031419.
Komnitsas, K., Zaharaki, D., Pyliotis, I., Vamvuka, D., Bartzas, G., 2015. Assessment of pistachio shell biochar quality and its potential for adsorption of heavy metals. Waste Biomass Valorization 6, 805–816. https://doi.org/10.1007/s12649-015-9364-5.
Komnitsas, K.A., Zaharaki, D., 2016. Morphology of modified biochar and its potential for phenol removal from aqueous solutions. Front. Environ. Sci. 4 https://doi.org/10.3389/fenvs.2016.00026.
Kovalakova, P., Cizmas, L., McDonald, T.J., Marsalek, B., Feng, M., Sharma, V.K., 2020. Occurrence and toxicity of antibiotics in the aquatic environment: a review. Chemosphere 251, 126351. https://doi.org/10.1016/j.chemosphere.2020.126351.
Krasucka, P., Pan, B., Sik Ok, Y., Mohan, D., Sarkar, B., Oleszczuk, P., 2021. Engineered biochar – a sustainable solution for the removal of antibiotics from water. J. Chem. Eng. 405, 126926 https://doi.org/10.1016/j.cej.2020.126926.
Lago, B.C., Silva, C.A., Melo, L.C.A., de Morais, E.G., 2021. Predicting biochar cation exchange capacity using Fourier transform infrared spectroscopy combined with partial least square regression. Sci. Total Environ. 794, 148762 https://doi.org/10.1016/j.scitotenv.2021.148762.
Lehmann, J., Joseph, S., 2015. Biochar for Environmental Management: Science, Technology and Implementation, Second edition. Routledge, Taylor & Francis Group, London ; New York.
Li, Y., Taggart, M.A., McKenzie, C., Zhang, Z., Lu, Y., Pap, S., Gibb, S., 2019. Utilizing low-cost natural waste for the removal of pharmaceuticals from water: mechanisms, isotherms and kinetics at low concentrations. J. Clean. Prod. 227, 88–97. https://doi.org/10.1016/j.jclepro.2019.04.081.
Liu, H., Zhang, J., Ngo, H.H., Guo, W., Wu, H., Guo, Z., Cheng, C., Zhang, C., 2015. Effect on physical and chemical characteristics of activated carbon on adsorption of trimethoprim: mechanisms study. RSC Adv. 5, 85187–85195. https://doi.org/10.1039/C5RA17968H.
Liu, W., Wang, J., Richard, T.L., Hartley, D.S., Spatari, S., Volk, T.A., 2017. Economic and life cycle assessments of biomass utilization for bioenergy products. Biofuels, Bioprod. Bioref. 11, 633–647. https://doi.org/10.1002/bbb.1770.
Mallaki, M., Fatehi, R., 2014. Design of a biomass power plant for burning date palm waste to cogenerate electricity and distilled water. Renew. Energy 63, 286–291. https://doi.org/10.1016/j.renene.2013.09.036.
McBride, M.B., 1994. Environmental Chemistry of Soils. Oxford University Press, New York.
Muter, O., Pērkons, I., Bartkevičs, V., 2019. Removal of pharmaceutical residues from wastewater by woodchip-derived biochar. DWT 159, 110–120. https://doi.org/10.5004/dwt.2019.24108.
Ndoun, M.C., Elliott, H.A., Preisendanz, H.E., Williams, C.F., Knopf, A., Watson, J.E., 2021. Adsorption of pharmaceuticals from aqueous solutions using biochar derived from cotton gin waste and guayule bagasse. Biochar 3, 89–104. https://doi.org/10.1007/s42773-020-00070-2.
Novak, J.M., Lima, I., Xing, B., Gaskin, J.W., Steiner, C., Das, K.C., Ahmedna, M., Rehrah, D., Watts, D.W., Busscher, W.J., Schomberg, H., 2009. Characterization of designer biochar produced at different temperatures and their effects on a loamy sand. AES 3.
Parikh, S.J., Goyne, K.W., Margenot, A.J., Mukome, F.N.D., Calderón, F.J., 2014. Soil chemical insights provided through vibrational spectroscopy. In: Advances in Agronomy. Elsevier, pp. 1–148. https://doi.org/10.1016/B978-0-12-800132-5.00001-8.
Peiris, C., Gunatilake, S.R., Mlsna, T.E., Mohan, D., Vithanage, M., 2017. Biochar based removal of antibiotic sulfonamides and tetracyclines in aquatic environments: a critical review. Bioresour. Technol. 246, 150–159. https://doi.org/10.1016/j.biortech.2017.07.150.
Ritchie, H., Roser, M., 2022. Water use and stress [WWW document]. URL. https://ourworldindata.org/water-use-stress. (Accessed 18 May 2022).
Sapkota, A.R., 2019. Water reuse, food production and public health: adopting transdisciplinary, systems-based approaches to achieve water and food security in a changing climate. Environ. Res. 171, 576–580. https://doi.org/10.1016/j.envres.2018.11.003.
Scholes, R.J., 2020. The future of semi-arid regions: a weak fabric unravels. Climate 8, 43. https://doi.org/10.3390/cli8030043.
Sizirici, B., Fseha, Y.H., Yildiz, I., Delclos, T., Khaleel, A., 2021. The effect of pyrolysis temperature and feedstock on date palm waste derived biochar to remove single and multi-metals in aqueous solutions. Sustain. Environ. Res. 31, 9. https://doi.org/10.1186/s42834-021-00083-x.
Stylianou, M., Christou, A., Michael, C., Agapiou, A., Papanastasiou, P., Fatta-Kassinos, D., 2021. Adsorption and removal of seven antibiotic compounds present in water with the use of biochar derived from the pyrolysis of organic waste feedstocks. J. Environ. Chem. Eng. 9, 105868 https://doi.org/10.1016/j.jece.2021.105868.
Sun, B., Lian, F., Bao, Q., Liu, Z., Song, Z., Zhu, L., 2016. Impact of low molecular weight organic acids (LMWOAs) on biochar micropores and sorption properties for sulfamethoxazole. Environ. Pollut. 214, 142–148. https://doi.org/10.1016/j.envpol.2016.04.017.
Sun, T., Levin, B.D.A., Schmidt, M.P., Guzman, J.J.L., Enders, A., Martínez, C.E., Muller, D.A., Angenent, L.T., Lehmann, J., 2018. Simultaneous quantification of electron transfer by carbon matrices and functional groups in pyrogenic carbon. Environ. Sci. Technol. 52, 8538–8547. https://doi.org/10.1021/acs.est.8b02340.
Szabo, D., Coggan, T.L., Robson, T.C., Currell, M., Clarke, B.O., 2018. Investigating recycled water use as a diffuse source of per- and polyfluoroalkyl substances (PFASs) to groundwater in Melbourne, Australia. Sci. Total Environ. 644, 1409–1417. https://doi.org/10.1016/j.scitotenv.2018.07.048.
Tahir, A.H.F., Al-Obaidy, A.H.M.J., Mohammed, F.H., 2020. Biochar from date palm waste, production, characteristics and use in the treatment of pollutants: a review. IOP Conf. Ser.: Mater. Sci. Eng. 737, 012171 https://doi.org/10.1088/1757-899X/737/1/012171.
Teixidó, M., Pignatello, J.J., Beltrán, J.L., Granados, M., Peccia, J., 2011. Speciation of the ionizable antibiotic sulfamethazine on black carbon (biochar). Environ. Sci. Technol. 45, 10020–10027. https://doi.org/10.1021/es202487h.
Tomczyk, A., Sokołowska, Z., Boguta, P., 2020. Biochar physicochemical properties: pyrolysis temperature and feedstock kind effects. Rev. Environ. Sci. Biotechnol. 19, 191–215. https://doi.org/10.1007/s11157-020-09523-3.
Wang, J., Chu, L., Wojnárovits, L., Takács, E., 2020. Occurrence and fate of antibiotics, antibiotic resistant genes (ARGs) and antibiotic resistant bacteria (ARB) in municipal wastewater treatment plant: an overview. Sci. Total Environ. 744, 140997 https://doi.org/10.1016/j.scitotenv.2020.140997.
Wang, X., Sato, T., Xing, B., 2006. Competitive sorption of pyrene on wood chars. Environ. Sci. Technol. 40, 3267–3272. https://doi.org/10.1021/es0521977.
Zhao, Z., Wu, Q., Nie, T., Zhou, W., 2019. Quantitative evaluation of relationships between adsorption and partition of atrazine in biochar-amended soils with biochar characteristics. RSC Adv. 9, 4162–4171. https://doi.org/10.1039/C8RA08544G.
Zheng, H., Wang, Z., Zhao, J., Herbert, S., Xing, B., 2013. Sorption of antibiotic sulfamethoxazole varies with biochars produced at different temperatures. Environ. Pollut. 181, 60–67. https://doi.org/10.1016/j.envpol.2013.05.056.
Zhu, X., He, M., Sun, Y., Xu, Z., Wan, Z., Hou, D., Alessi, D.S., Tsang, D.C.W., 2022. Insights into the adsorption of pharmaceuticals and personal care products (PPCPs) on biochar and activated carbon with the aid of machine learning. J. Hazard. Mater. 423, 127060 https://doi.org/10.1016/j.jhazmat.2021.127060.